Investigation of laser-induced grating spectroscopy of O_2 for accurate temperature measurements towards applications in harsh environments

Hot, Dina; Sahlberg, Anna Lena; Alden, Marcus; Li, Zhongshan

Published in:
Journal of Raman Spectroscopy

DOI:
10.1002/jrs.6099

2021

Document Version:
Publisher's PDF, also known as Version of record

EDINBURGH INSTRUMENTS

50 YEARS 1971-2021

PRECISION RAMAN

Best-in-class Raman microscopes for research and analytical requirements backed with world-class customer support and service.

edinst.com

Received: 30 November 2020 | Revised: 6 March 2021 | Accepted: 6 March 2021

DOI: 10.1002/jrs.6099

SPECIAL ISSUE - RESEARCH ARTICLE

Journal of RAMAN SPECTROSCOPY WILEY

Investigation of laser-induced grating spectroscopy of O_2 for accurate temperature measurements towards applications in harsh environments

Dina Hot | **Anna-Lena Sahlberg** | **Marcus Alden** | **Zhongshan Li**

Division of Combustion Physics, Lund University, Lund, Sweden

Correspondence
Anna-Lena Sahlberg, Division of Combustion Physics, Lund University, P.O. Box 118, S-221 00, Lund, Sweden.
Email: anna-lena.sahlberg@forbrf.lth.se

Funding information
H2020 European Research Council; Knut and Alice Wallenberg Foundation; Swedish Energy Agency; Swedish Research Council

Abstract

We present an in-depth investigation of laser-induced grating spectroscopy (LIGS) for temperature measurements in practical applications using a narrow-band dye laser with 760 nm wavelength and a pulse duration of 8 ns as the source for the pump beams creating the laser-induced grating. The pump laser wavelength was set to be either resonant with the ${}^{R}Q(5)$ transition from the $b^1\Sigma_g^+\ (v'=0) \leftarrow X^3\Sigma_g^-\ (v''=0)$ band of O_2 for generation of thermal LIGS or nonresonant for generation of purely electrostrictive LIGS. Signals were generated in ambient air as well as in high-pressure or high-temperature dry air mixtures. Pump laser irradiances up to 11 GW/cm^2 were used, which resulted in strong electrostrictive contribution to the overall LIGS signals at atmospheric pressure, with a low thermal contribution due to the weak absorption by the singlet O_2 $\left(b^1\Sigma_g^+, v'=0\right)$. The advantage and disadvantage of thermal or electrostrictive LIGS for temperature measurements are discussed, as well as potential applications in high-pressure environments. Furthermore, the precision of the temperature measurement is discussed by comparing different analysis methods.

KEYWORDS

electrostrictive, LIGS, oxygen, temperature, thermal

1 | INTRODUCTION

Temperature is a key parameter in combustion processes. A large focus of laser diagnostics in combustion is directed towards accurate and precise temperature measurements in situ with high spatial and temporal resolution. Several spectroscopic techniques have been developed and applied for temperature measurements in various combustion situations, such as Coherent Antistokes Raman Scattering (CARS),[1–4] Rayleigh scattering,[5] Raman scattering,[6] laser-induced fluorescence (LIF),[6–9] two-line atomic fluorescence (TLAF),[10–12] degenerate four-wave mixing,[13–15] and many more. The field of laser techniques for combustion diagnostics has been reviewed several times.[16–18]

Laser-induced grating spectroscopy (LIGS) has emerged in recent decades as a promising candidate for temperature measurements in combustion. The LIGS signal is rich in information, as the shape of the signal simultaneously holds information on temperature,[19–22]

pressure,[21,23] velocity,[24–27] and molecular relaxation rates.[28–30] In particular, LIGS has great potential for temperature measurements in high-pressure environments, since unlike most other laser techniques, the signal intensity and the precision in the temperature measurement improve at higher pressures.[31] This makes LIGS an attractive technique for temperature measurements in high-pressure applications such as gas turbines and combustion engines. Latzel et al.[21] demonstrated the first application of LIGS for temperature measurements in high-pressure flames. LIGS for temperature measurements have been demonstrated under diesel engine conditions[32] and in an optical engine using simultaneous LIGS and two-color planar LIF.[33] Pressure measurements in an engine using thermal LIGS were demonstrated by Sahlberg et al.[23]

In a typical LIGS experiment, two coherent pump beams from a pulsed laser are overlapped and create an interference pattern in the intersection region. The signal can be generated from two fundamental phenomena. Absorption of the pump laser radiation by molecules in the measurement volume, and subsequent thermalization of the energy due to molecular collisions, results in a transient density modulation and thus refractive index spatial modulation. Electrostriction, in turn, generates a modulation in the gas density by compression of the molecules by the strong electric fields in the pump laser beams. Both of these processes lead to the formation of a laser-induced grating (LIG). The signal is generated by aligning a continuous wave probe laser to cross the LIG at the Bragg angle and detecting the light that is Bragg scattered off the LIG. Rapid density variations lead to the formation of a standing acoustic wave across the LIG. This results in oscillations in the LIGS signal, directly proportional to the sound speed in the medium, which in turn depends on the gas temperature. In cases where there is a strong absorption and thermalization of the absorbed energy, a weak pump laser is generally used and the electrostrictive part of the LIGS signal can sometimes be neglected. On the other hand, in the absence of any absorption, a relatively strong pump laser will be applied to generate a pure electrostrictive LIGS signal.[31]

The choice for using thermal or electrostrictive LIGS signals is generally determined by the availability of laser system and molecular species with absorption lines at the appropriate wavelength. Acetone or toluene has frequently been used as absorbers in LIGS experiments at 266 nm.[33–35] However, this method is limited to measurements before combustion since the tracers are consumed during combustion. For measurements in the burned zone of flames, absorption lines of nitric oxide (NO) around 226 nm[36] or water around 3 μm[37,38] that are naturally present in flames have been utilized. However, NO is only naturally present in sufficient quantity in high-temperature flames, and water requires a suitable midinfrared laser source.

The advantage of electrostrictive LIGS measurements is that the pump laser wavelength does not need to be tuned to absorption lines in the gas.[39–41] The disadvantage of electrostrictive LIGS compared to thermal LIGS is that a much stronger laser intensity is required to generate electrostrictive LIGS signals. For this reason, the fundamental output from a Nd:YAG laser (at 1064 nm) has traditionally been used for electrostrictive LIGS measurements, because of the ease of generating high power at this wavelength.[22,26,40,42] However, too high laser power can be a limitation in some applications due to the risk of laser-induced breakdown and damage to optical components. Electrostrictive LIGS have been used for measurements of temperature in atmospheric pressure flames.[22] Förster et al.[32] recently demonstrated both thermal and electrostrictive LIGS experiments under diesel engine conditions, proving that the electrostrictive LIGS signal could provide temperature measurements also in the burned zone of the gas.

Absorption by the spin-forbidden and hence weak rovibronic transition of O_2 $\left(b^1\Sigma_g^+, v'=0 \leftarrow X^3\Sigma_g^-, v''=0\right)$ can be used for generation of thermal LIGS signals. It has been used for fundamental studies of the mechanics of energy transfer in the singlet O_2 $\left(b^1\Sigma_g^+\right)$ band under different conditions.[28–30,43] In this work, we examine the potential of both thermal and electrostrictive LIGS at this wavelength for temperature measurements in practical applications. A narrow-band dye laser with 760 nm wavelength, 8 ns pulse duration, and up to 60 mJ pulse energy operating at 10 Hz was used as the source for the pump beams. The pump laser wavelength was adjusted to be either resonant with the singlet O_2 $\left(b^1\Sigma_g^+, v'=0\right)$ ${}^RQ(5)$ transition for generation of thermal LIGS signals or nonresonant for generation of purely electrostrictive LIGS signals. The dependence of the signal shape and intensity on the pump laser energy, temperature, and pressure have been studied. The advantage and disadvantage of thermal or electrostrictive LIGS for temperature measurements are discussed from an application-based point of view, that is, for potential applications for temperature measurements in high-pressure environments such as gas turbines.

2 | THEORY

The theory of LIGS has been reported by several groups (see, e.g., previous studies[26,31,44–46]). In a typical LIGS setup, two pulsed pump laser beams with wavelength

λ_{pump} are crossed in an angle θ. Coherent interference between the pump beams generates a fringe pattern of alternating intensity with the characteristic grating spacing Λ, which is given by

$$\Lambda = \frac{\lambda_{pump}}{2\sin(\theta/2)} \tag{1}$$

If the pump laser beams are resonant with a transition in the molecules present in the crossing region, the molecules will be excited along the interference fringes of high laser intensity in the measurement volume. Molecular collisions will de-excite the molecules and transfer the absorbed laser energy into thermal energy, which forms a periodic variation in temperature in the gas in the measurement point. The rapid changes in temperature cause a density modulation, which results in two counter-propagating acoustic waves perpendicular to the fringe planes, that is, a standing wave. The temperature and density modulation together with the standing acoustic wave causes a modulation of the refractive index in the measurement volume, that is, a laser-induced thermal grating (LITG). Due to the standing acoustic wave, the LITG will oscillate at the frequency f_{osc} which depends on the speed of sound, v_s, and the grating spacing as

$$f_{osc} = \Lambda / v_s \tag{2}$$

In addition to the resonant absorption, a modulation of the molecular density in the measurement volume can be introduced by electrostriction (the tendency of a material to vary its density in presence of an electric field gradient). The density modulation caused by electrostriction leads to the formation of a standing wave in the measurement volume and produces a nonresonant laser-induced electrostrictive grating (LIEG). The LIEGS signal will oscillate at twice the oscillation frequency f_{osc} compared to a LITGS signal with the same grating spacing.[47]

If the pump laser is resonant with a molecular absorption line and both the thermal and electrostrictive effects are present, then a combined LITGS and LIEGS signal will be formed. The LIEG is more dependent on a strong pump laser intensity compared to the LITG. If the resonant absorption is strong and the pump laser intensity is low, the LIEG might be negligible.

The formation and time evolution of the LIG is probed by a continuous wave (CW) probe laser beam. The wavelength λ_{probe} can be chosen arbitrarily, and the probe beam is aligned to cross the LIG at the Bragg angle θ_B, which is given by (for first-order diffraction)

$$\sin(\theta_B) = \frac{\lambda_{probe}}{2\Lambda} \tag{3}$$

The LIGS signal is formed by Bragg diffraction of the probe beam off the LIG. The signal intensity scales linearly with the probe laser power and quadratically with the pump laser intensity (until saturation or laser-induced breakdown occurs).

2.1 | Temperature measurements using LIGS

The LIGS signal can be directly used to measure the speed of sound v_s in the measurement volume by measuring the oscillation frequency f_{osc}. The gas temperature T can be calculated from the speed of sound as

$$T = \frac{v_s^2}{R_u(\gamma/M_{gas})} = \frac{(\Lambda/f_{osc})^2}{R_u(\gamma/M_{gas})} \tag{4}$$

where R_u is the universal gas constant, $\gamma = c_p/c_v$ is the ratio of specific heats at constant pressure and volume, and M_{gas} is the mean molecular weight of the gas. Thus, the gas temperature can be directly calculated from the oscillation frequency, provided the gas composition is known or can be estimated.

2.2 | Acoustic damping and thermal diffusivity

The acoustic waves decay exponentially due to viscous damping. The time of decay is given by the acoustic damping time, τ_a, which can be calculated as

$$\tau_a = 2\left(\frac{\Lambda}{2\pi}\right)^2 \left\{\frac{1}{\rho}\left[\frac{4}{3}\mu + (\gamma - 1)\cdot\frac{\kappa}{c_p}\right]\right\}^{-1} \tag{5}$$

where κ is the thermal conductivity, ρ is the density, c_p is the specific heat at constant pressure, μ is the dynamic viscosity, and γ is the specific heat ratio.

Since the measurement volume is not infinite in size, the acoustic waves will travel out of the volume during the lifetime of the LIG. The oscillations will then also decay exponentially due to the acoustic transit time τ_{tr}[26] which depends on the beam radius w at the measurement volume and the speed of sound as

$$\tau_{tr} = \frac{w}{\sqrt{2}v_s\cos(\theta/2)} \approx \frac{w}{\sqrt{2}v_s} \tag{6}$$

In many practical LIGS experiments using focused pump laser beams, the measurement volume is small enough

TABLE 1 Gas constants for dry air at 296 K and pressures 1–7 bar, together with the calculated acoustic damping time and thermal diffusion time assuming a grating spacing of $\Lambda = 11.5$ μm

P (bar)	κ (mW/m·K)	ρ (kg/m3)	c_p (kJ/kg·K)	μ (μPa·s)	γ	χ (mm2/s)	τ_a (μs)	τ_{th} (μs)
1	25.7	1.18	1.0065	18.385	1.4018	21.69	0.23	0.15
2	25.73	2.35	1.0081	18.4	1.4036	10.84	0.45	0.31
3	25.77	3.53	1.0098	18.415	1.4055	7.22	0.68	0.46
4	25.8	4.71	1.0114	18.43	1.4073	5.41	0.9	0.62
5	25.84	5.89	1.0131	18.445	1.4091	4.33	1.12	0.77
6	25.88	7.07	1.0147	18.461	1.4109	3.61	1.35	0.93
7	25.92	8.25	1.0164	18.476	1.4127	3.09	1.57	1.08

that the acoustic transit time is much smaller than the acoustic damping. If this is the case, the viscous damping can be neglected.

The stationary thermal part of the LIG grating decays exponentially according to thermal diffusion. The time constant for this decay, τ_{th}, is given by

$$\tau_{th} = \left(\frac{\Lambda}{2\pi}\right)^2 \chi^{-1} \tag{7}$$

where the thermal diffusivity $\chi = \kappa/\rho c_p$. Table 1 shows the values of the gas constants for dry air at room temperature and at different pressures,[48] as well as the calculated thermal diffusion and acoustic damping times, assuming a grating spacing of 11.5 μm. Table 2 shows the same values for 1 bar and at different temperatures.

2.3 | LIGS simulation model

The time evolution of a thermal LIG is strongly influenced by the time scale of the thermalization of the absorbed pump laser energy. The shape of the resulting LIGS signal depends on the characteristic time τ_m in which the energy transfer occurs. If $\tau_m \ll \tau_L$, where τ_L is the laser pulse duration, the signal is assumed to be "instantaneous."

A model for simulations of the LITGS signals generated from excitation of the singlet O_2 $\left(b^1\Sigma_g^+\right)$ band has been developed by Hemmerling and Kozlov.[29] They presented a model describing the temporal evolution of a LIG signal created by the interference of population, electrostrictive, and thermal contributions, where the thermal contribution is divided into "instantaneous," "fast," and "slow" energy transfer processes. Depending on the gas density (the frequency of molecular collisions), these processes contribute differently; at low gas densities, the main contribution is from instantaneous energy transfer, while the fast and slow transfer gains more importance at higher densities.[29]

It has been shown[29] that the "slow" processes, which mainly occur from vibrational transitions, are negligible for the pressure range 1–7 bar. Therefore, in this paper we assume the energy transfer to occur in two steps: one "instantaneous" transfer, followed by a "fast" energy transfer characterized by the time constant τ_f. In this case, the time evolution of the LIGS signal S_{LIGS} can be modeled as

$$\begin{aligned} S_{LIGS} \propto \Bigg\{ & M_i\left[\cos(2\pi f_{osc}t)\exp\left(-t/\tau_a-(t/\tau_{tr})^2\right)-\exp(-t/\tau_{th})\right] \\ & + M_f\left[\left(\frac{1}{k_f}\sin(2\pi f_{osc}t)\right)\exp\left(-t/\tau_a-(t/\tau_{tr})^2\right)-\frac{\left[\exp(-t/\tau_{th})-\exp\left(-t/\tau_f\right)\right]}{\tau_f\left(1/\tau_f-1/\tau_{th}\right)}\right] \\ & + M_e\sin(2\pi f_{osc}t)\exp\left(-t/\tau_a-(t/\tau_{tr})^2\right)\Bigg\}^2 \end{aligned} \tag{8}$$

where the constants M_i, M_f, and M_e represent the relative contributions of instantaneous, fast/slow, or electrostrictive processes, respectively. The constant k_f is defined

TABLE 2 Gas constants for dry air at 1 bar and 296–700 K together with the calculated acoustic damping time and thermal diffusion time assuming a grating spacing of $\Lambda = 11.5$ μm

T (K)	κ (mW/m·K)	ρ (kg/m^3)	c_p (kJ/kg·K)	μ (μPa·s)	γ	χ (mm^2/s)	τ_a (ns)	τ_{th} (ns)
296	25.7	1.18	1.0065	18.39	1.4018	21.69	230	150
423	34.26	0.829	1.0169	23.95	1.3946	40.63	120	80
700	50.85	0.497	1.0752	34.27	1.3646	95.09	53	35

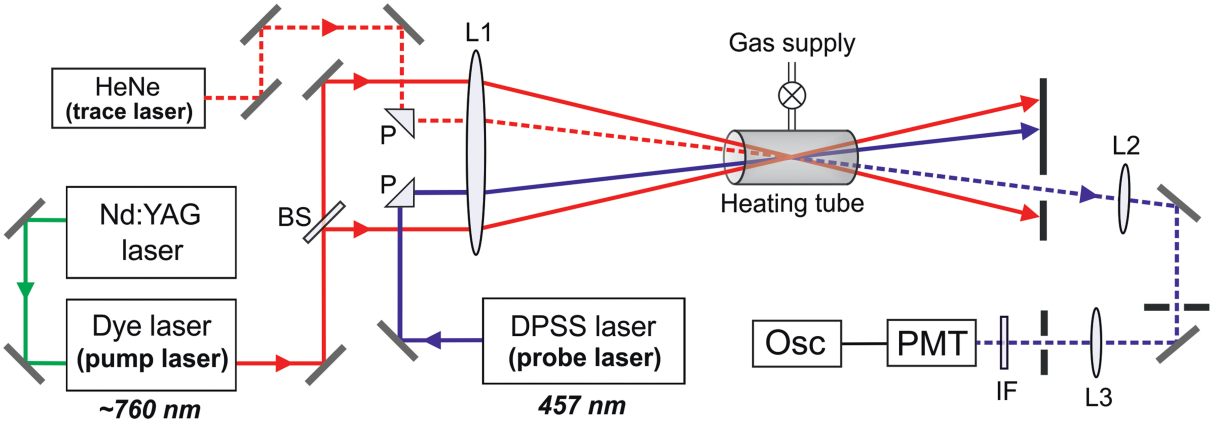

FIGURE 1 Schematic overview of the laser-induced grating spectroscopy (LIGS) experimental arrangement. The measurements were performed in room air, in heated gas flows of dry air (depictured), and in dry air at elevated pressures using a high-pressure cell. The focal lengths of the plano-convex fused silica lenses L1–L3 are 300, 500, and 300 mm, respectively. The other abbreviations denote BS: beam splitter, P: quartz prism, IF: interference filter 457.9 ± 2 nm

as $k_f = 2\pi f_{osc}\tau_f$, and it is assumed that $k_f \gg 1\text{-}\tau_a/\tau_f$. If the laser wavelength is off-resonance, M_i and M_f are zero and the electrostrictive LIGS signal is given only by the last term in Equation 8. In the limited range of temperatures and pressures studied in this paper, this model was sufficient for an accurate simulation of the LIGS signal shapes.

2.4 | Spectral line notation of oxygen

The rotational levels of O_2 are described by the angular momenta K and J, where K represents the rotational angular momentum and J is the sum of the rotational (K) and spin angular momenta.[49–51] The spectral line notation used here is ${}^{\Delta K}\Delta J(K'')$ where K'' and J'' are the quantum numbers of the initial rotational level in the ground state $X^3\Sigma_g^-(v''=0)$. For example, the absorption line ${}^RQ(5)$ represents the ${}^RQ$-branch line with $K''=5$ where $\Delta J=0$ and $\Delta K=1$.

3 | EXPERIMENTAL ARRANGEMENT

Figure 1 illustrates a schematic view of the experimental setup. A dye laser (Sirah, PRSC-D-18, operating on LDS765 dye) pumped by the second harmonic output of a pulsed injection-seeded Nd:YAG laser (Spectra Physics, PRO 290–10, 10 Hz) was used to generate tuneable laser radiation with wavelength around 760 nm. The pulse duration is 8 ns, and the linewidth of the laser radiation has a full-width half maximum (FWHM) <0.04 cm^{-1}. This laser radiation served as pump laser in the LIGS configuration. The maximum output pulse energy of the laser is around 60 mJ.

The pump laser beam was split into two pump beams by a 50:50 beam splitter and was focused and crossed using a plano-convex fused silica lens with a focal length of $f = 300$ mm. A crossing angle of 3.7° was used, which resulted in formation of a LIG with a grating spacing of 11.5 μm. This geometry was chosen in order to create a LIG with largest achievable grating spacing in order to produce LIGS signals with long durations, while maintaining high spatial resolution. A larger grating spacing leads to longer signal duration (due to the increased decay time constant of thermal diffusion according to Equation 7). It also leads to lower oscillation frequency; however, the increased signal duration is larger than the decrease in oscillation frequency, so larger grating spacing leads to more observable oscillation peaks in the signal and thereby increases the measurement precision.

A CW diode-pumped solid state (DPSS) laser (Laserglow Tech., LRS-0457) operating at 457 nm with an output power of 170 mW was used to probe the dynamics of the grating. The probe laser was aligned to intersect the LIG at the Bragg angle of 1.1°, and a HeNe laser beam was used to facilitate the alignment of the signal beam towards the detector. The signal beam was collimated and detected using a photomultiplier tube (PMT, Hamamatsu, H6780-04) connected to an oscilloscope (LeCroy, WaveRunner 6,100, 1 GHz). An interference filter with central wavelength 457.9 ± 2 nm was used in front of the PMT to suppress any scattered light from the pump laser.

The LIGS measurements were performed in known gas environments which included room-temperature humid air and dry air at pressures 1–7 bar using a pressurized gas cell equipped with sapphire windows for optical access. The pressure measurements were performed at room temperature. In addition to that, LIGS signals at atmospheric pressure and temperatures between room temperature and 710 K were recorded in dry air flows in a heating tube. A thermocouple of type K was used to measure the heated gas flow temperature. The gas flow was controlled by mass flow controllers (Bronkhorst).

4 | RESULTS

4.1 | LIGS signals recorded in room air

Figure 2 shows the LIGS signals recorded in room air at 295 K with 35% humidity both off-resonance and on-resonance with the absorption line $^{R}Q(5)$ of the $b^1\Sigma_g^+\ (v'=0) \leftarrow X^3\Sigma_g^-\ (v''=0)$ band of O_2. The humidity in the air will affect the strength of the thermal LIGS, since the concentration of water vapor in the air strongly affects the quenching that forms the thermal LIG. The recorded LIGS signals presented below are an average of 200 laser shots unless stated otherwise. The ellipsoid probe volume was estimated to be 1.5 mm long with a diameter of 75 μm. The pulse energy of the pump beams was around 50 mJ during these measurements, which corresponds to a laser irradiance around 14 GW/cm^2. This was more than sufficient to create a LIEG.

The nonresonant LIGS signal presented in Figure 2a was recorded in room air at 761.16 nm. The inset in the figure shows the Fourier transform of the signal, where the peak in the power spectrum reveals an oscillation frequency around 58 MHz. This corresponds to the frequency originating from a LIEG with grating spacing 11.5 μm. Figure 2b shows the resonant signal recorded on the $^{R}Q(5)$ absorption line of O_2 at 761.139 nm. This signal exhibits a higher intensity of the even-numbered oscillation peaks (marked with arrows) compared to the nonresonant signal, which indicates a contribution from a LITG. Two observable features are present in the power spectrum (see inset of Figure 2b). Just like for the nonresonant LIEGS signal, an oscillation frequency peak around 58 MHz is present and thus indicating a strong electrostrictive contribution.

Furthermore, a distinct dip occurs at 29 MHz, which corresponds to the oscillation frequency from the LITG contribution. It is more common to observe a peak in the power spectrum at the oscillation frequency, instead of a dip. It is possible that this occurs because the conditions in this measurement caused a destructive interference effect between the acoustic waves from the different LITGS and LIEGS frequencies in the power spectrum. It could be that the conditions in this experiment were just right to create a destructive interference between the two

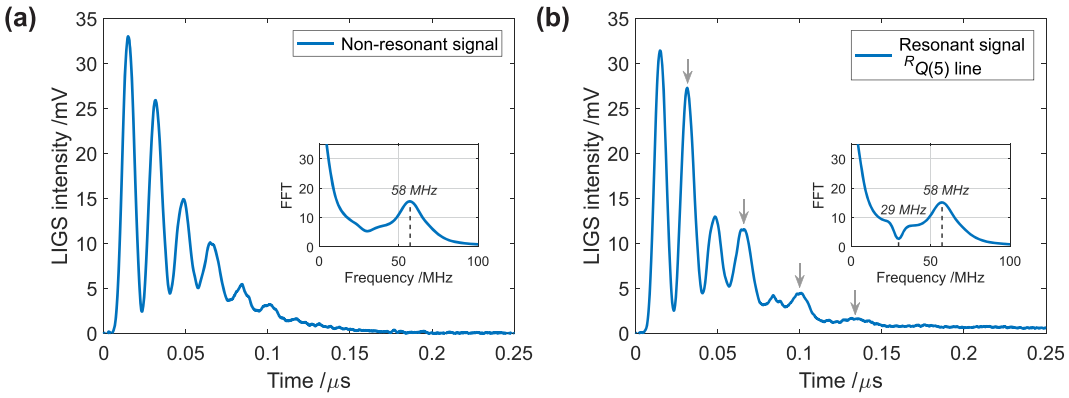

FIGURE 2 Laser-induced grating spectroscopy (LIGS) signals recorded at 295 K in room air (a) off resonance at 761.16 nm and (b) on-resonance with the RQ(5) absorption line of the b1 Σg + (v′ = 0)←X3 Σg − (v″ = 0) band of O_2. The insets show the power spectrum of the signals obtained by Fourier transform and reveal the oscillation frequency of the signals. The arrows in (b) indicate the even-numbered oscillation peaks where the thermal contribution is visible

acoustic waves, LIEG and LITG, that reduce the amplitude of the signal at the fundamental frequency of the LITGS. The dip could also be caused by a negative interference between the oscillation peak and the continuous slope background in the Fourier transform. Further experiments are required to determine if there are other conditions in LIGS experiments that can produce the same results. The small dip in the power spectrum in Figure 2a, which should be a pure LIEGS signal, is probably caused by some weak absorption in the pressure-broadened wing of a nearby absorption line that generates a very small thermal signal.

Figure 3 shows the peak LIGS signal dependence on pump laser irradiance. The nonresonant (LIEGS) signals were recorded at 762.4 nm, and the measurements were performed in room air at 295 K with 35% humidity. The pump laser energy was measured before the beam splitter, and the ellipsoid area of the probe volume was calculated based on the alignment geometry. For the given probe area, a laser irradiance up to 11 GW/cm^2 (corresponding to 40 mJ/pulse) was achieved, which resulted in strong LIEGS signals with a signal-to-noise ratio better than 2000. Even when the laser wavelength was tuned to an O_2 absorption line, the electrostrictive contribution dominated the signal. Therefore, the signal dependence upon pump laser irradiance was only performed for nonresonant LIEGS signals. These results differ from previous work by Kozlov et al.[29,30] and Hubschmid et al.,[28,43] where their measurements were performed in pure O_2 gas environment or with admixtures of selected molecular species, such as CO_2 and H_2. They also had lower pump laser irradiances since they used lower pulse energies for the pump laser and a focusing lens with longer focal length ($f = 1000$ mm), which results in a larger probe volume. This resulted in dominating thermal LIGS signals with low or negligible electrostrictive contribution.

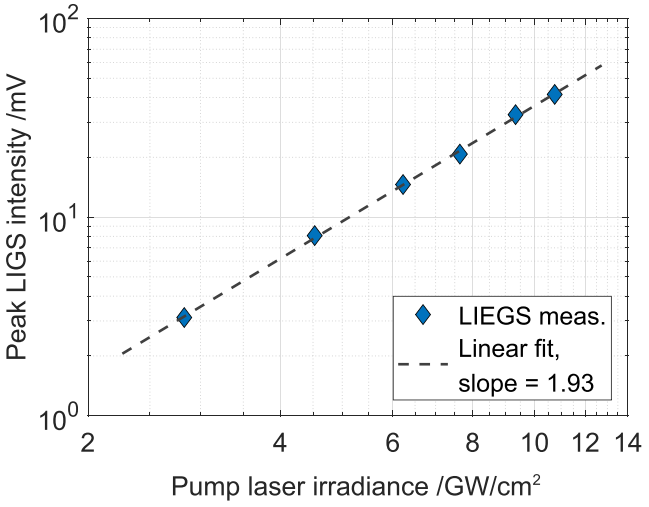

FIGURE 3 Signal dependence upon the pump laser irradiance for the nonresonant laser-induced electrostrictive grating (LIEGS) signals recorded at 762.4 nm in room air at 295 K. The slope indicates approximately a quadratic dependence of the signal on the pump laser intensity

4.2 | LIGS signals at different pressures

The resonant (LITGS) signal shown in Figure 4a was recorded at 761.139 nm, which is resonant with the $^RQ(5)$ transition in the singlet O_2 $\left(b^1\Sigma_g^+, v' = 0\right)$ band. The nonresonant (LIEGS) signal shown in Figure 4b was recorded at 762.4 nm. The ellipsoid probe volume during these measurements was estimated to be 125 µm with a length of 2.7 mm. The measurements were performed in dry air in the high-pressure cell, pressurized between

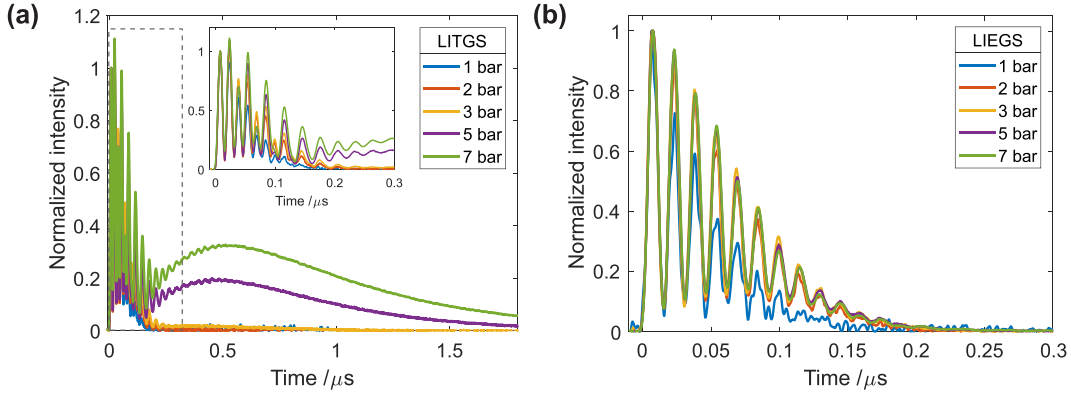

FIGURE 4 Laser-induced grating spectroscopy (LIGS) signals recorded in dry air at different pressures and at 295 K. (a) Resonant LITGS signals recorded on the RQ(5) O_2 line. The inset shows a zoom on the first oscillating part of the signal. (b) Nonresonant laser-induced electrostrictive grating (LIEGS) signal recorded at 762.4 nm. The intensity of the signals has been normalized to the first peak

1 and 7 bar and at 295 K. The intensity of the signals has been normalized to the intensity of the first oscillation peak.

The inset in Figure 4a shows the first, oscillating part of the LITGS signals. At 1 bar, the thermal part of the signal is very weak and the electrostrictive part is dominant. As the pressure increases, the thermal part of the signal grows, and the even-numbered oscillation peaks increase in intensity compared to the odd-numbered peaks. The long "tail" rising in the signals at higher pressures occurs due to the noninstantaneous, fast energy transfer mechanism, which becomes more dominant as the pressure increases. The decay of the signal tail depends on the thermal diffusivity of the gas. Measuring the decay of the signal can be used for pressure measurements.[23]

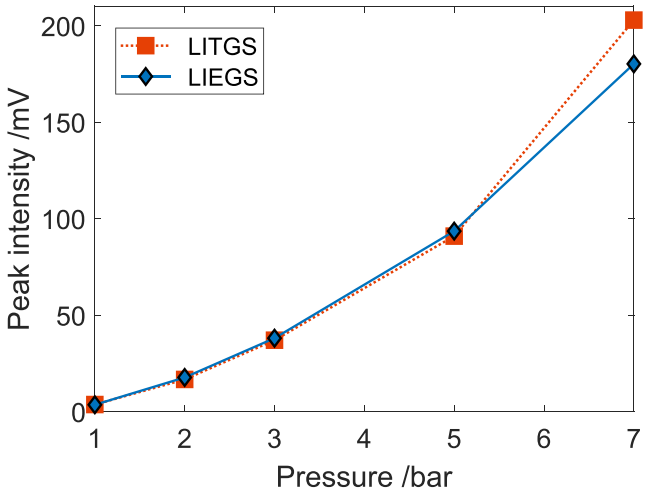

FIGURE 5 The maximum peak signal intensity of the resonant LITGS (red) and nonresonant laser-induced electrostrictive grating (LIEGS) (blue) signals at different pressures that are presented in Figure 4

Unlike the resonant LITGS signal, the nonresonant LIEGS signal shape is almost identical over all pressures. This is because the shape of the electrostrictive signal is not affected by collisions and energy transfers. Instead, the signal duration depends on the decay of the acoustic waves. This is affected by two factors: the acoustic transit out of the measurement volume and the acoustic damping.[52] The acoustic transit time for the measurements in Figure 4 is around 0.13 μs. Table 1 shows the calculated acoustic damping time for dry air at pressures between 1 and 7 bar. The acoustic damping is fastest at 1 bar, and the damping time increases at higher pressures. This is the reason the LIEGS signal in Figure 4b decays faster at 1 bar, where the acoustic damping is comparable to the acoustic transit time. At higher pressures, where the acoustic damping is slower, the decay is mainly defined by the acoustic transit time.

Figure 5 shows the maximum peak signal intensity at different pressures for the resonant LITGS signal (red) and the nonresonant LIEGS signals (blue) presented in Figure 4. The peak intensity was observed to increase up to 45 times when increasing the pressure from 1 to 7 bar. Since the peak intensity is mainly dependent on the first electrostrictive oscillation, the LITGS and LIEGS signals have very similar signal intensities. As the pressure increases, the LITGS signal gets slightly higher intensity since the second oscillation peak gets higher due to an increase in the thermal contribution to the signal.

4.2.1 | Simulations of measured signals at different pressure

Figure 6 shows the simulated and measured resonant LITGS and nonresonant LIEGS signals at 5 bar. The

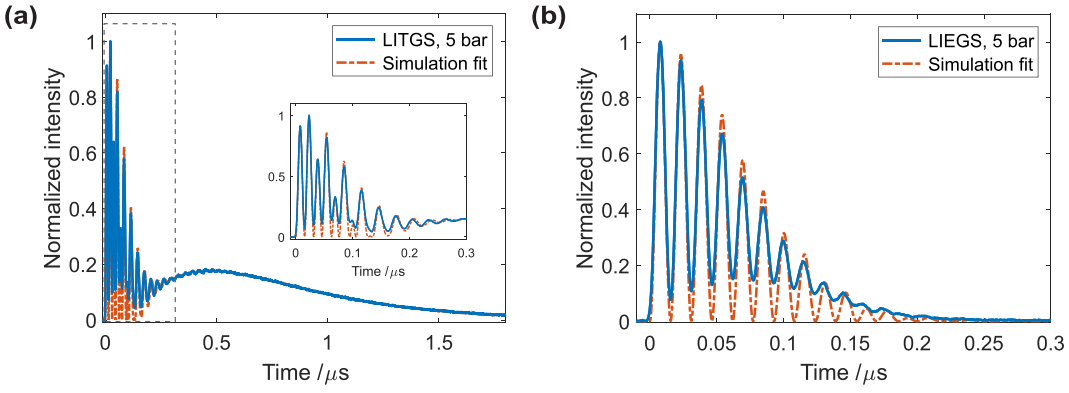

FIGURE 6 Simulated (red dashed line) and measured (blue line) (a) resonant LITGS and (b) nonresonant laser-induced electrostrictive grating (LIEGS) signal at 5 bar in dry air. The inset in (a) shows the first oscillating part of the signal. The intensity has been normalized to the strongest oscillation peak

signal was recorded in dry air in the high-pressure cell, pressurized up to 5 bar. The inset in Figure 6a zooms in on the first oscillating part of the signal. Every second peak has a higher intensity, because the electrostrictive part of the signal oscillates at twice the frequency of the thermal signal and its contribution adds to the thermal signal. Figure 6b shows the nonresonant LIEGS signal at 5 bar compared with the simulation. Due to pressure broadening of the O_2 spectrum at higher pressures, it is possible that there is some absorption adding a small thermal LIG part to the electrostrictive LIGS signal.

One thing that is immediately clear in Figure 6 is that the contrast of the oscillations in the measured LIGS signals is less than for the simulated signals. The model in Equation 8[29,53] assumes that the oscillations originate from a perfect standing acoustic wave generated by the pump beams in the measurement volume. In the ideal case, for signals with a strong electrostrictive part, the contrast of the oscillations should be 100%, as shown in the simulations. However, the model does not take the effects of sound propagation into account. A standing acoustic wave causes oscillations in the LIGS signal. A propagating acoustic wave, however, leads to a nonoscillating contribution to the LIGS signal which grows and decays at the same rate as the oscillatory part. Thus, the propagation of the sound waves out of the measurement volume leads to a signal which is increasingly less modulated, as has been shown by Stampanoni-Panariello et al.[26] Another thing that can decrease the contrast is a nonoptimal alignment. If all three pump and probe beams are perfectly aligned, the probe beam scatters mainly from the center of the measurement volume. However, a slight misalignment leads to scattering from the edges of the volume where the interference of the acoustic waves is poor, leading to a propagating wave being present as well.[26] If the probe beam is larger than the pump beams in the measurement volume, this can also lead to interference from scattering at the edges of the beam, which decreases the contrast of the oscillations. In conclusion, the cause of the discrepancy in the contrast of oscillations between measurement and simulation in Figure 6 is likely a combination of tightly focused beams, sound propagation, and a less than optimal overlap between the probe beam and the pump beams. However, a qualitative comparison using this simple simulation model can still be used for accurate determination of the oscillation frequency.

4.3 | Temperature measurements

Figure 7a shows the normalized nonresonant LIEGS signals (average of 200 single-shot signals) recorded at 762.4 nm and at three different temperatures in an atmospheric pressure dry air flow. The ellipsoid probe volume is estimated to be 1.5 mm long with a diameter of 75 μm. The Fourier transform of the signals presented in Figure 7b shows how the oscillation frequency in the signals increases as the temperature increases. The oscillation frequency is determined by identifying the position of the peak in the power spectrum. Since the thermal contribution to the overall LIGS is negligible in dry air flows at atmospheric pressure, as was shown in Figure 2, only the nonresonant LIEGS signal was analyzed for the temperature measurement.

As the temperature increases, the signals decay more quickly, due to the acoustic waves traveling faster out of the interaction region. The signal at 710 K (dotted line) contains only three clear oscillation peaks before the signal disappears. This results in a wider

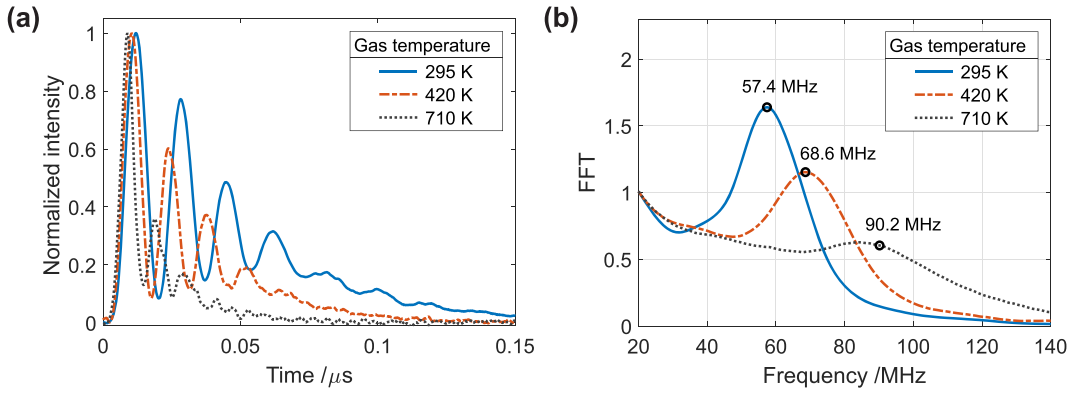

FIGURE 7 (a) Normalized laser-induced electrostrictive grating (LIEGS) signals at different temperatures in a dry air flow at atmospheric pressure. (b) The corresponding Fourier transform of the signals, with the oscillation frequency identified by the circles

frequency peak in the power spectrum superimposed on a slope, which decreases the precision of the oscillation frequency measurement. Because of this, it is difficult to determine the correct oscillation frequency (and corresponding gas temperature) in the short-lived high-temperature signals. A more precise temperature measurement was achieved by fitting a simulated LIGS signal to the measurement in order to determine the frequency.

4.3.1 | Signal shape

Comparing the LIEGS signal at 1 bar in the high-pressure cell (Figure 4b) with the LIEGS signal in the room temperature dry air flow (Figure 7a), it is clear that the signal in the high-pressure cell contains more oscillations and has a higher contrast of the oscillations. The decay of the oscillations is mainly limited by the acoustic transit time, which depends on the width of the pump beams at the crossing point. By placing an iris in the pump beam path, the size of the pump laser beams before the focusing lens can be reduced. Since the size of the focused laser beams is inversely proportional to the laser beam size before the lens, reducing the laser beam size leads to less tightly focused beams and thus an increased size of the measurement volume. This, in turn, increases the number of oscillations in the signals and also improves contrast of the oscillations due to better pump/probe overlap. However, reducing the laser beam size in this way also decreases the intensity in the pump beams, which lowers the signal intensity, and increases the size of the probe volume, which affects the spatial resolution. Therefore, there is a trade-off between the signal intensity, the spatial resolution, and the signal shape when optimizing the alignment. During the pressure measurements, where the signal intensity was generally very strong, the pump beam size before the focusing lens was reduced to half of its original size (4 mm), in order to achieve the best signal shape. The diameter of the ellipsoid probe volume for the measurements in the high-pressure gas cell is estimated to be 125 μm, which is a significant increase over the probe volume diameter of 75 μm for the air flow measurements. Because of this, the recorded signals at 1 bar in the pressure gas cell (Figure 4b) have better signal shape but reduced signal-to-noise ratio compared to the signals in the room temperature dry air flow (Figure 7a). However, during the high-temperature measurements, where the signal intensity at elevated temperatures was very low, the alignment was optimized for maximum signal strength instead. Using higher laser intensity and a tighter focus led to a higher signal intensity but a less optimal signal shape.

4.3.2 | Single-shot precision at different temperatures

The average shot-to-shot variation in the measured single-shot LIGS signal intensity was around ±23% in our measurements. Figure 8 shows the simulated fit for some single-shot LIEGS signals at 710 K. The temperature is calculated for each signal from the fitted oscillation frequency, and the precision is given by the 95% confidence interval of the fitting process.

The fit is relatively good for the signals presented in Figure 8a,b in terms of the derived temperature. However, for signals with lower intensity as shown in Figure 8c,d, the precision of the fitted simulations is limited since the position of the oscillation peaks is difficult to determine due to the low signal-to-noise ratio of the recorded signals. This affects the determination of the oscillation frequency and thus the temperature. Hence, these results indicate the detection limit of the current setup for high-temperature measurements at atmospheric pressure.

Table 3 displays the averaged measured temperature from 100 single-shot signals, and the precision is shown as the standard deviation of the derived temperatures from each single-shot signal. The Fourier transform of the signal and the fitted simulations are both used to extract the temperature. For the Fourier transform method, the peak is identified by smoothing out the noise inherent in the spectrum and finding the maximum of the peak in the power spectrum within a reasonably chosen interval. The Fourier transform method is faster and less computationally expensive, but the fitted simulations give better precision in the shot-to-shot variation in the derived temperatures. At 710 K, the fitted temperature also gives a more accurate value than the Fourier transform.

The precision in the fitted simulation method depended on how the signals were analyzed. As it can be seen in Figure 8, some of the recorded single-shot signals had too low signal-to-noise ratio to give a reliable fit for the oscillation frequency. If all signals are included in the measurement, the shot-to-shot temperature had a standard deviation of ±70 K. If we exclude the single-shot signals with intensities below the detection limit for a reliable simulation fit, the precision is improved to ±44 K.

In situations where the expected temperature interval is known, the temperature can be quickly and relatively reliably extracted from the Fourier transform even for short-lived signals, but for situations where the expected temperature variation is large, this is an unreliable method. Fitting a simulated LIGS signal to the measurements is more reliable. However, fitting simulated LIGS

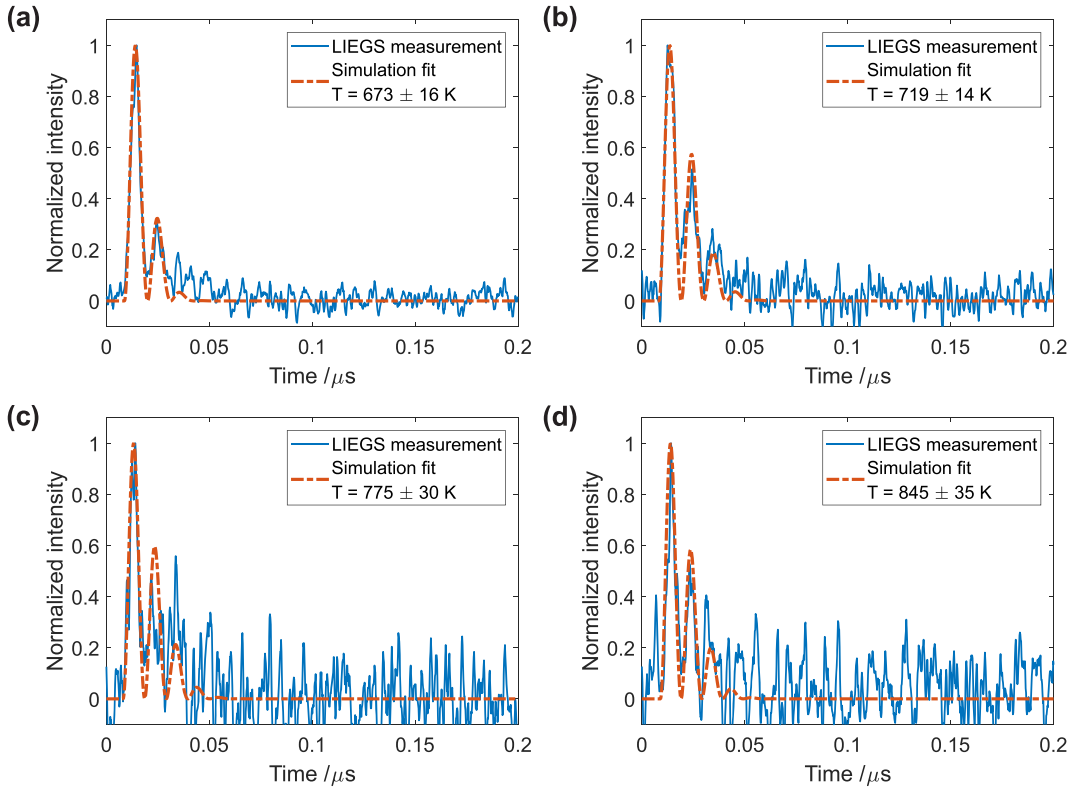

FIGURE 8 Selected single-shot nonresonant laser-induced electrostrictive grating (LIEGS) signals recorded at 762.4 nm in heated dry air flow at atmospheric pressure, together with fitted simulations and corresponding determined temperature. The gas flow temperature was measured with a thermocouple to be around 710 K. The precision is given by the confidence interval of the fitted oscillation frequency. Panels (a) and (b) show signals with a good fit for the temperature, while panels (c) and (d) have too low signal-to-noise ratio to extract a reliable temperature

TABLE 3 The average single-shot nonresonant LIEGS temperature for the different temperature gas flows in the heating tube

	Thermocouple temperature		
Analysis method	**295 K**	**418 K**	**710 K**
Fourier transform	295 ± 7 K	436 ± 26 K	732 ± 90 K
Fit simulations	295 ± 4 K	446 ± 13 K	710 ± 70 K

Note: The temperature was determined using the Fourier transform method or the fit simulation method, respectively. The precision in each value is given by the standard deviation of the temperature derived from 100 single-shots.
Abbreviation: LIEGS, laser-induced electrostrictive grating.

TABLE 4 The average of the LIGS temperature for 100 single-shot signals, recorded at 1 and 5 bar in the high-pressure cell

Analysis method	**1 bar**	**5 bar**
Fourier transform		
LIEGS	295 ± 7.1 K	295 ± 2.9 K
LITGS	293 ± 6.3 K	295 ± 2.3 K
Fit simulations		
LIEGS	295 ± 4.2 K	294 ± 1.8 K
LITGS	296 ± 3.3 K	296 ± 1.3 K

Note: The temperature was determined using the Fourier transform method and the fit simulation method, respectively. The precision in each value is given by the standard deviation of the temperature derived from 100 single-shots.
Abbreviations: LIEGS, laser-induced electrostrictive grating; LIGS, laser-induced grating spectroscopy.

signals will not work in cases where signal-to-noise ratio is too low to identify more than one oscillation peak.

4.3.3 | Single-shot precision at different pressures in room temperature

As has been shown many times before, the precision of LIGS temperature measurements is strongly related to the signal duration and number of oscillations in the signal. Table 4 compares the single-shot precision in determining the temperature from the LIGS signals at 1 and 5 bar, respectively. The precision is given as the standard deviation of the shot-to-shot variation in LIGS temperature determined from 100 single-shots.

As can be deduced from Table 4, the precision in determining the oscillation frequency, and hence the temperature, is significantly better at 5 bar compared to 1 bar, because of the longer signal duration and more oscillations visible. This is partly due to the stronger signals at 5 bar and partly because the alignment was optimized for a better signal shape. It can also be seen that the precision is similar for the nonresonant LIEGS signals and the resonant LITGS signals. This is expected since the signal intensity and the duration of the oscillating part of the signals are similar. Also, the precision is much better when using the simulation method compared to the Fourier transform method.

5 | CONCLUSIONS

Thermal and electrostrictive LIGS has been investigated for the potential application for temperature measurements by resonant and nonresonant excitation of the weak $b^1\Sigma_g^+ (v'=0) \leftarrow X^3\Sigma_g^- (v''=0)$ band of O_2 around 760 nm. Pump laser irradiances up to 11 GW/cm^2 were used throughout the investigation, which resulted in strong electrostrictive contributions to the overall LIGS signals. Even resonant signals at atmospheric pressures resulted in a dominating electrostrictive contribution with a weak thermal contribution. Therefore, the temperature measurements at atmospheric pressure were performed with nonresonant LIGS between room temperature and up to 710 K. In order to retrieve the temperature, the oscillation frequency in the LIGS signals was extracted, both through direct Fourier transform reading and through a simulation fit to the signal. While the former method is straight forward to use, it has a relatively larger standard deviation in frequency for low intensity signals due to the difficulty to determine the position of the frequency peak in the power spectrum. The method of using a simulation fit to the LIGS signals is then preferred since the oscillation frequency can be identified with higher precision. The electrostrictive LIGS signal dominates at atmospheric pressure, but at higher pressures the thermal contribution to the LIGS signal gains in intensity. Analysis of the oscillation frequency at different pressures, both through direct Fourier transform and the simulation fit to the signal, also shows that the precision of the temperature measurement improves with higher pressures due to the stronger signal intensities.

In conclusion, both thermal and electrostrictive LIGS have good potential for precise temperature measurements, especially at elevated pressures. The electrostrictive and thermal LIGS signals show very similar precision for temperature measurements, but the thermal signal also contains information about the thermal diffusivity of the medium which could potentially also be used for pressure measurements. The advantage of electrostrictive LIGS is that the laser wavelength can be chosen freely, which makes it easier to find a suitable high-power laser system. Potential application would be in high-pressure environments, for example, in the post flame zone in a high-pressure flame or gas turbine. In these kinds of applications, resonant O_2 LIGS can only be applied in environments where oxygen is present, that is, at fuel-lean conditions.

ACKNOWLEDGEMENTS

This work was supported by the Swedish Research Council (Vetenskapsrådet), the Swedish Energy Agency (Energimyndigheten) through the KC-CECOST project, the Knut and Alice Wallenberg Foundation (Knut och Alice Wallenbergs stiftelse) through the COCALD project, and the H2020 European Research Council (ERC) through the Advanced Grant TUCLA.

ORCID

Anna-Lena Sahlberg https://orcid.org/0000-0002-1239-1665

REFERENCES

[1] C. J. Kliewer, Y. Gao, T. Seeger, J. Kiefer, B. D. Patterson, T. B. Settersten, *Proc. Combust. Inst.* **2011**, *33*, 831.
[2] C. Brackmann, J. Bood, P.-E. Bengtsson, T. Seeger, M. Schenk, A. Leipertz, *Appl. Optics* **2002**, *41*, 564.
[3] R. L. Farrow, R. P. Lucht, W. L. Flower, R. E. Palmer, *Proc. Combust. Inst.* **1984**, *20*, 1307.
[4] M. Aldén, S. Wallin, *Appl. Optics* **1985**, *24*, 3434.
[5] P. Petersson, J. Olofsson, C. Brackman, H. Seyfried, J. Zetterberg, M. Richter, M. Alden, M. A. Linne, R. K. Cheng, A. Nauert, D. Geyer, A. Dreizler, *Appl. Optics* **2007**, *46*, 3928.
[6] A. T. Hartlieb, B. Atakan, K. Kohse-Hoinghaus, *Appl. Phys. B: Lasers Opt.* **2000**, *70*, 435.
[7] J. Kiefer, A. Meyerhoefer, T. Seeger, A. Leipertz, Z. S. Li, M. Alden, *J. Raman Spectrosc.* **2009**, *40*, 828.
[8] M. P. Lee, B. K. McMillin, R. K. Hanson, *Appl. Optics* **1993**, *32*, 5379.
[9] J. M. Seitzman, R. K. Hanson, P. A. Debarber, C. F. Hess, *Appl. Optics* **1994**, *33*, 4000.
[10] J. Borggren, I. S. Burns, A.-L. Sahlberg, M. Aldén, Z. Li, *Appl. Phys. B: Lasers Opt.* **2016**, *122*, 1.
[11] I. S. Burns, X. Mercier, M. Wartel, R. S. M. Chrystie, J. Hult, C. F. Kaminski, *Proc. Combust. Inst.* **2011**, *33*, 799.
[12] R. S. M. Chrystie, I. S. Burns, J. Hult, C. E. Kaminski, *Opt. Lett.* **2009**, *34*, 2492.
[13] Z. W. Sun, Z. S. Li, B. Li, M. Aldén, *J. Raman Spectrosc* **2011**, *42*, 1828.
[14] C. F. Kaminski, I. G. Hughes, G. M. Lloyd, P. Ewart, *Appl. Phys. B: Lasers Opt.* **1996**, *62*, 39.
[15] G. M. Lloyd, I. G. Hughes, R. Bratfalean, P. Ewart, *Appl. Phys. B: Lasers Opt.* **1998**, *67*, 107.

[16] K. Kohse-Höinghaus, *Prog. Energy Combust. Sci.* **1994**, *20*, 203.
[17] A. Ehn, J. Zhu, X. Li, J. Kiefer, *Appl. Spectrosc.* **2017**, *71*, 341.
[18] M. Aldén, J. Bood, Z. Li, M. Richter, *Proc. Combust. Inst.* **2011**, *33*, 69.
[19] A. Hayakawa, T. Yamagami, K. Takeuchi, Y. Higuchi, T. Kudo, S. Lowe, Y. Gao, S. Hochgreb, H. Kobayashi, *Proc. Combust. Inst.* **2019**, *37*, 1427.
[20] F. J. Förster, C. Crua, M. Davy, P. Ewart, *Exp. Fluids* **2017**, *58*, 87.
[21] H. Latzel, A. Dreizler, T. Dreier, J. Heinze, M. Dillmann, W. Stricker, G. M. Lloyd, P. Ewart, *Appl. Phys. B: Lasers Opt.* **1998**, *67*, 667.
[22] A. Stampanoni-Panariello, B. Hemmerling, W. Hubschmid, *Appl. Phys. B: Lasers Opt.* **1998**, *67*, 125.
[23] A. L. Sahlberg, A. Luers, C. Willman, B. A. O. Williams, P. Ewart, *Appl. Phys. B: Lasers Opt.* **2019**, *125*, 46.
[24] D. J. W. Walker, R. B. Williams, P. Ewart, *Opt. Lett.* **1998**, *23*, 1316.
[25] M. Neracher, W. Hubschmid, *Appl. Phys. B: Lasers Opt.* **2004**, *79*, 783.
[26] A. Stampanoni-Panariello, D. N. Kozlov, P. P. Radi, B. Hemmerling, *Appl. Phys. B: Lasers Opt.* **2005**, *81*, 101.
[27] F. J. Förster, S. Baab, G. Lamanna, B. Weigand, *Appl. Phys. B: Lasers Opt.* **2015**, *121*, 235.
[28] W. Hubschmid, B. Hemmerling, *Chem. Phys.* **2000**, *259*, 109.
[29] B. Hemmerling, D. N. Kozlov, *Chem. Phys.* **2003**, *291*, 213.
[30] D. N. Kozlov, V. D. Kobtsev, O. M. Stel'makh, V. V. Smirnov, *J. Exp. Theor. Phys.* **2013**, *117*, 36.
[31] J. Kiefer, P. Ewart, *Prog. Energy Combust. Sci.* **2011**, *37*, 525.
[32] F. Förster, C. Crua, M. Davy, P. Ewart, *Combust. Flame* **2019**, *199*, 249.
[33] B. Scott, C. Willman, B. Williams, P. Ewart, C. R. Stone, *SAE Int. J. Engines* **2017**, *10*, 2191.
[34] B. Williams, M. Edwards, R. Stone, J. Williams, P. Ewart, *Combust. Flame* **2014**, *161*, 270.
[35] B. Williams, P. Ewart, *Chem. Phys. Lett.* **2012**, *546*, 40.
[36] A. Luers, A.-L. Sahlberg, S. Hochgreb, P. Ewart, *Appl. Phys. B: Lasers Opt.* **2018**, *124*, 43.
[37] A.-L. Sahlberg, D. Hot, J. Kiefer, M. Aldén, Z. Li, *Proc. Combust. Inst.* **2017**, *36*, 4515.
[38] D. Hot, A.-L. Sahlberg, M. Aldén, Z. Li, *Proc. Combust. Inst.* **2020**. https://doi.org/10.1016/j.proci.2020.06.289
[39] W. Hubschmid, B. Hemmerling, A. Stampanoni-Panariello, *J. Opt. Soc. Am. B* **1995**, *12*, 1850.
[40] A. Stampanoni-Panariello, B. Hemmerling, W. Hubschmid, *Phys. Rev. A* **1995**, *51*, 655.
[41] B. Hemmerling, W. Hubschmid, D. N. Kozlov, A. Stampanoni, Proc. SPIE 3732, ICONO '98: laser spectroscopy and optical diagnostics: novel trends and applications in laser chemistry, biophysics, and biomedicine, **1999**, Doi: https://doi.org/10.1117/12.340005
[42] D. N. Kozlov, B. Hemmerling, A. Stampanoni-Panariello, *Appl. Phys. B: Lasers Opt.* **2000**, *71*, 585.
[43] W. Hubschmid, *Appl. Phys. B: Lasers Opt.* **2009**, *94*, 345.
[44] E. B. Cummings, *Opt. Lett.* **1994**, *19*, 1361.
[45] E. B. Cummings, I. A. Leyva, H. G. Hornung, *Appl. Optics* **1995**, *34*, 3290.
[46] P. H. Paul, R. L. Farrow, P. M. Danehy, *J. Opt. Soc. Am. B* **1995**, *12*, 384.
[47] D. E. Govoni, J. A. Booze, A. Sinha, F. F. Crim, *Chem. Phys. Lett.* **1993**, *216*, 525.
[48] NIST, REFPROP, **2020**, https://www.nist.gov/srd/refprop
[49] L. Herzberg, G. Herzberg, *Astrophys. J.* **1947**, *105*, 353.
[50] H. D. Babcock, L. Herzberg, *Astrophys. J.* **1948**, *108*, 167.
[51] L. R. Brown, C. Plymate, *J. Mol. Spectrosc.* **2000**, *199*, 166.
[52] D. N. Kozlov, J. Kiefer, T. Seeger, A. P. Fröba, A. Leipertz, *J. Phys. Chem. B* **2014**, *118*, 14493.
[53] D. N. Kozlov, J. Kiefer, T. Seeger, A. P. Fröba, A. Leipertz, *J. Phys. Chem. B* **2011**, *115*, 8528.

How to cite this article: D. Hot, A.-L. Sahlberg, M. Alden, Z. Li, *J Raman Spectrosc* **2021**, *52*(9), 1569. https://doi.org/10.1002/jrs.6099